# The SCUBA–2 Cosmology Legacy Survey: blank-field number counts of 450μm-selected galaxies and their contribution to the cosmic infrared background

J. E. Geach[1]⋆, E. L. Chapin[2,3,4], K. E. K. Coppin[1], J. S. Dunlop[5], M. Halpern[2], Ian Smail[6], P. van der Werf[7], S. Serjeant[8], D. Farrah[9], I. Roseboom[5], T. Targett[5], V. Arumugam[5], V. Asboth[3], A. Blain[10], A. Chrysostomou[3,11], C. Clarke[12], R. J. Ivison[5,13], S. L. Jones[10], A. Karim[6], T. Mackenzie[2], R. Meijerink[7,14], M. J. Michałowski[5], D. Scott[2], J. Simpson[6], A. M. Swinbank[6], D. Alexander[6], O. Almaini[15], I. Aretxaga[16], P. Best[5], S. Chapman[17], D. L. Clements[18], C. Conselice[15], A. L. R. Danielson[6], S. Eales[19], A. C. Edge[6], A. Gibb[3], D. Hughes[16], T. Jenness[3], K. K. Knudsen[20], C. Lacey[6], G. Marsden[2], R. McMahon[21], S. Oliver[12], M. J. Page[22], J. A. Peacock[5], D. Rigopoulou[23,24], E. I. Robson[13], M. Spaans[14], J. Stevens[11], T. M. A. Webb[1], C. Willott[25], C. D. Wilson[26], M. Zemcov[27]

[1] *Department of Physics, Ernest Rutherford Building, 3600 rue University, McGill University, Montréal, QC, H3A 2T8, Canada*
[2] *Department of Physics & Astronomy, University of British Columbia, 6224 Agricultural Road, Vancouver, BC, V6T 1Z1, Canada*
[3] *Joint Astronomy Centre 660 N. A'ohoku Place University Park Hilo, Hawaii 96720, USA*
[4] *XMM SOC, ESAC, Apartado 78, 28691 Villanueva de la Canada, Madrid, Spain*
[5] *Institute for Astronomy, University of Edinburgh, Royal Observatory, Blackford Hill, Edinburgh EH9 3HJ*
[6] *Institute for Computational Cosmology, Department of Physics, Durham University, South Road, Durham, DH1 3LE*
[7] *Leiden Observatory, Leiden University, P.O. box 9513, 2300 RA Leiden, The Netherlands*
[8] *Robert Hooke Building, Department of Physical Sciences, The Open University, Milton Keynes, MK7 6AA*
[9] *Virginia Polytechnic Institute & State University Department of Physics, MC 0435, 910 Drillfield Drive, Blacksburg, VA 24061, USA*
[10] *Department of Physics & Astronomy, University of Leicester, University Road, Leicester, LE1 7RH*
[11] *Centre for Astrophysics Research, Science & Technology Research Institute, University of Hertfordshire, Hatfield, AL10 9AB*
[12] *Astronomy Centre, Department of Physics and Astronomy, University of Sussex, Brighton BN1 9QH*
[13] *UK Astronomy Technology Centre, Royal Observatory, Blackford Hill, Edinburgh EH9 3HJ*
[14] *Kapteyn Institute, University of Groningen, P.O. Box 800, 9700 AV Groningen, The Netherlands*
[15] *School of Physics and Astronomy, University of Nottingham, University Park, Nottingham, NG9 2RD*
[16] *Instituto Nacional de Astrofísica Óptica y Electrónica, Calle Luis Enrique Erro No. 1, Sta. Ma. Tonantzintla, Puebla, México*
[17] *Department of Physics and Atmospheric Science, Dalhousie University Halifax, NS, B3H 3J5, Canada*
[18] *Astrophysics Group, Imperial College London, Blackett Laboratory, Prince Consort Road, London, SW7 2AZ*
[19] *Cardiff School of Physics and Astronomy, Cardiff University, Queens Buildings, The Parade, Cardiff, CF24 3AA*
[20] *Department of Earth and Space Science, Chalmers University of Technology, Onsala Space Observatory, SE-43992 Onsala, Sweden*
[21] *Institute of Astronomy, University of Cambridge, Madingley Road, Cambridge, CB3 OHA*
[22] *Mullard Space Science Laboratory, University College London, Holmbury St Mary Dorking, Surrey RH5 6NT*
[23] *Department of Physics, University of Oxford, Keble Road, Oxford, OX1 3RH*
[24] *Space Science & Technology Department, Rutherford Appleton Laboratory, Chilton, Didcot, Oxfordshire, OX11 0QX*
[25] *Canadian Astronomy Data Centre, National Research Council Canada, 5071 West Saanich Road, Victoria, BC, V9E 2E7, Canada*
[26] *Department of Physics and Astronomy, McMaster University Hamilton, ON, L8S 4M1, Canada*
[27] *Astronomy Department, California Institute of Technology, MC 367-17 1200 East California Blvd., Pasadena, CA 91125, USA*

29 November 2012

**ABSTRACT**

The first deep blank-field $450\mu$m map ($1\sigma \approx 1.3$ mJy) from the SCUBA–2 Cosmology Legacy Survey (S2CLS), conducted with the James Clerk Maxwell Telescope (JCMT) is presented. Our map covers 140 arcmin$^2$ of the Cosmological Evolution Survey (COSMOS) field, in the footprint of the *Hubble Space Telescope* (*HST*) Cosmic Assembly Near-Infrared Deep Extragalactic Legacy Survey (CANDELS). Using 60 submillimetre galaxies (SMGs) detected at $\geqslant 3.75\sigma$, we evaluate the number counts of $450\mu$m-selected galaxies with flux densities $S_{450} > 5$ mJy. The $8''$ JCMT beam and high sensitivity of SCUBA–2 now make it possible to directly resolve a larger fraction of the cosmic infrared background (CIB, peaking at $\lambda \sim 200\mu$m) into the individual galaxies responsible for its emission than has previously been possible at this wavelength. At $S_{450} > 5$ mJy we resolve $(7.4 \pm 0.7) \times 10^{-2}$ MJy sr$^{-1}$ of the CIB at $450\mu$m (equivalent to $16 \pm 7\%$ of the absolute brightness measured by the *Cosmic Background Explorer* at this wavelength) into point sources. A further $\sim 40\%$ of the CIB can be recovered through a statistical stack of $24\mu$m emitters in this field, indicating that the majority ($\approx 60\%$) of the CIB at $450\mu$m is emitted by galaxies with $S_{450} > 2$ mJy. The average redshift of $450\mu$m emitters identified with an optical/near-infrared counterpart is estimated to be $\langle z \rangle = 1.3$, implying that the galaxies in the sample are in the ultraluminous class ($L_{\rm IR} \approx 1.1 \times 10^{12} {\rm L}_\odot$). If the galaxies contributing to the statistical stack lie at similar redshifts, then the majority of the CIB at $450\mu$m is emitted by galaxies in the LIRG class with $L_{\rm IR} > 3.6 \times 10^{11} {\rm L}_\odot$.

**Key words:** galaxies: high-redshift, active, evolution, cosmology: observations, submillimetre: galaxies

# 1  INTRODUCTION

Fifteen years have passed since the first 'submillimetre galaxies' (SMGs) were discovered (Smail, Ivison & Blain 1997; Barger et al. 1998; Hughes et al. 1998), a high-redshift population ($z \sim 2 - 3$, Chapman et al. 2005; Aretxaga et al. 2007; Wardlow et al. 2011) with ultraluminous ($10^{12} {\rm L}_\odot$) levels of bolometric emission, the bulk of which is emitted in the far-infrared (FIR) and redshifted to submillimetre wavelengths at $z > 1$. The power of submillimetre surveys for exploring the formation phase of massive galaxies was recognised before their discovery (e.g. Blain & Longair 1993; Dunlop et al. 1994), and since their discovery, their importance as a cosmologically significant population has been established by many studies (e.g. Smail et al. 2002; Dunlop et al. 2004; Ivison et al. 2000, 2005, 2010; Coppin et al. 2008; Michałowski et al. 2010; Hainline et al. 2011; Hickox et al. 2012; and see Dunlop et al. 2011 for a review). As such, SMGs provide challenging tests for models of galaxy formation, both in detailed 'zoomed' simulations as well as in cosmological theatres (Baugh et al. 2005; Davé et al. 2010). However, our view of the SMG population remains incomplete.

In ground-based work, the majority of SMGs have – so-far – mainly been selected in the $850\mu$m or 1 mm atmospheric windows (e.g. Coppin et al. 2006; Weiss et al. 2009; Austermann et al. 2010; Scott et al. 2010), but this is far removed from the peak of the Cosmic infrared background (CIB), which is at $\lambda \sim 200\mu$m (Fixsen et al. 1998). The next available window closer to the CIB peak is at $450\mu$m, but the transmission of this window is just at best 50% of the $850\mu$m window, making $450\mu$m SMG surveys challenging from ground-based sites. Submillimetre surveys working closer to the CIB peak are essential if we are to identify the galaxies responsible for its emission; the $S_{450}/S_{850}$ colours of sources identified in the very deepest (lensing assisted) submillimetre surveys (Blain et al. 1999; Knudsen et al. 2008) suggests that these sources con-

tribute less than half of the CIB at $450\mu$m (and therefore even less at the actual peak).

The Balloon-borne Large Aperture submillimetre Telescope (BLAST, Pascale et al. 2008) made progress by conducting a low resolution submillimetre survey from the stratosphere at 250, 350 and $500\mu$m (Pascale et al. 2008; Devlin et al. 2009; Glenn et al. 2010). This work was taken forward by the *Herschel Space Observatory*, which carries an instrument that images in the same wavelength ranges as BLAST (the Spectral and Photometric Imaging Receiver; SPIRE), and has mapped hundreds of square degrees of the sky at $250$–$500\mu$m in a combination of panoramic and deep cosmological surveys (Eales et al. 2010, Oliver et al. 2010, 2012). However, the low resolution and high confusion limits of *Herschel* (FWHM$\sim 0.5'$ at $500\mu$m, $\sigma_{\rm con} \approx 7$ mJy beam$^{-1}$, Nguyen et al. 2010) limit the fraction of the CIB that can be directly resolved, with 15% resolved into individual galaxies at $250\mu$m and 6% at $500\mu$m (Clements et al. 2010; Glenn et al. 2010; Béthermin et al. 2012a). Thus, there remains work to be done in identifying the galaxies that emit the CIB, and thus finally complete the census of dust-obscured activity in the Universe and its role in galaxy evolution.

Advances in submillimetre imaging technology are just now allowing us to take up the search once more, taking advantage of higher resolution possible with large terrestrial telescopes, and improved sensitivity and mapping capability in submillimetre detector arrays. The SCUBA–2 camera is the state-of-the-art in submillimetre wide-field instrumentation (Holland et al. 2006). The camera, now mounted on the 15 m James Clerk Maxwell Telescope (JCMT), consists of 5000 pixels in both $450\mu$m and $850\mu$m detector arrays with an $8' \times 8'$ field-of-view ($16\times$ that of its predecessor, SCUBA). The increase in pixel number is the reward of developments in submillimetre detector technology; SCUBA–2 utilizes superconducting transition edge sensors (TES) to detect submillimetre photons, with multiplexed superconducting quantum interference device (SQUID) amplifiers handling read-out, analogous to an optical CCD. SCUBA–2 offers the capability to efficiently

$^\star$ E-mail: jimgeach@physics.mcgill.ca
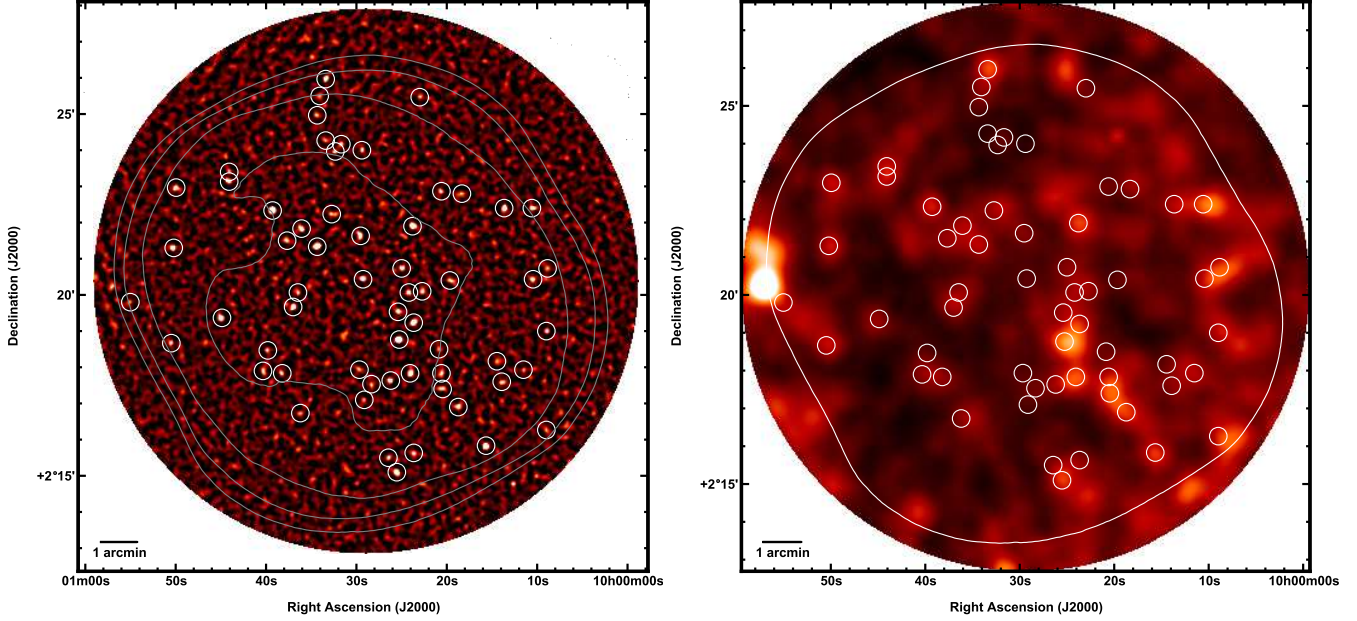
**Figure 1.** (left) SCUBA–2 450$\mu$m signal-to-noise ratio map of the COSMOS/CANDELS field. The map has been scaled to emphasize the visibility of 60 sources detected at $>3.75\sigma$ significance (circled). The grey contours show the variation in the noise level, and are at $\sigma_{450} = 2, 3, 4, 5$ mJy beam$^{-1}$ (the solid angle bounded by the $\sigma_{450} = 5$ mJy beam$^{-1}$ contour is $\Omega \approx 140$ arcmin$^2$). (right) *Herschel*-SPIRE 500$\mu$m image of the same region, from the HerMES survey (Oliver et al. 2012). This map has been slightly smoothed with a Gaussian kernel to improve presentation. We show the limiting $\sigma_{450} = 5$ mJy beam$^{-1}$ contour used for 450$\mu$m detection in the SCUBA–2 map and the position of the same galaxies in the left panel. This illustrates the ability of SCUBA–2 to push below the *Herschel* confusion limit at similar wavelengths, resolving confused emission into individual galaxies.

map large (degree-scale) areas, and has the sensitivity to simultaneously achieve deep (confusion limited) maps at both 450$\mu$m and 850$\mu$m. At 450$\mu$m, the resolution attainable with the JCMT is a factor $\sim5\times$ finer than the 500$\mu$m resolution of *Herschel*, and the confusion limit is $\sim7\times$ fainter.

Here we present results from early science observations of one of the seven components of the JCMT Legacy Survey[1]: the SCUBA–2 Cosmology Legacy Survey (S2CLS)[2]. The goal of the S2CLS is to fully exploit SCUBA–2's mapping capabilities for the purpose of exploring the high redshift Universe. The S2CLS will cover several well-studied extragalactic 'legacy' fields, including the United Kingdom Infrared Deep Sky Survey Ultra Deep Survey field (UDS), the Cosmological Evolution field (COSMOS), the Extended Groth Strip, and the Great Observatories Origins Deep Survey (North) fields. We present the deepest blank-field map at 450$\mu$m yet produced (in the COSMOS field), and measure the flux distribution and abundance of the extragalactic sources revealed within it. In §2 we describe the observations and data reduction technique, in §3 we calculate the 450$\mu$m number counts and evaluate the contribution to the CIB at 450$\mu$m. We briefly discuss and summarize our findings in §4 & §5.

## 2 OBSERVATIONS AND DATA REDUCTION

Observations were conducted in Band 1 weather conditions ($\tau_{225\,\mathrm{GHz}} < 0.05$) over 22 nights between 23$^{\mathrm{rd}}$ January and 20$^{\mathrm{th}}$ May 2012 totalling 50 hours of on-sky integration. The mapping centre of the SCUBA–2 COSMOS/CANDELS field is $\alpha = 10^{\mathrm{h}}$

10$^{\mathrm{m}}$ 29.8$^{\mathrm{s}}$, $\delta = 02°$ 15′ 01.6″, chosen to be in the footprint of the *Hubble Space Telescope* CANDELS (Grogin et al. 2011; Koekemoer et al. 2011)[3]. A standard 3 arcmin diameter 'daisy' mapping pattern was used, which keeps the pointing centre on one of the four SCUBA–2 sub-arrays at all times during exposure.

### 2.1 Map making

Individual 30 min scans are reduced using the dynamic iterative map-maker of the SMURF package (Jenness et al. 2011; Chapin et al. 2012 in prep). Raw data are first flat-fielded using ramps bracketing every science observation, scaling the data to units of pW. The signal recorded by each bolometer is then assumed to be a linear combination of: (a) a common mode signal dominated by atmospheric water and ambient thermal emission; (b) the astronomical signal (attenuated by atmospheric extinction); and finally (c) a noise term, taken to be the combination of any additional signal not accounted for by (a) and (b). The dynamic iterative map maker attempts to solve for these model components, refining the model until convergence is met, an acceptable tolerance has been reached, or a fixed number of iterations has been exhausted (in this case, 20). This culminates in time-streams for each bolometer that should contain only the astronomical signal, corrected for extinction, plus noise. The signal from each bolometer's time stream is then re-gridded onto a map, according to the scan pattern, with the contribution to a given pixel weighted according to its time-domain variance (which is also used to estimate the $\chi^2$ tolerance in the fit derived by the map maker).
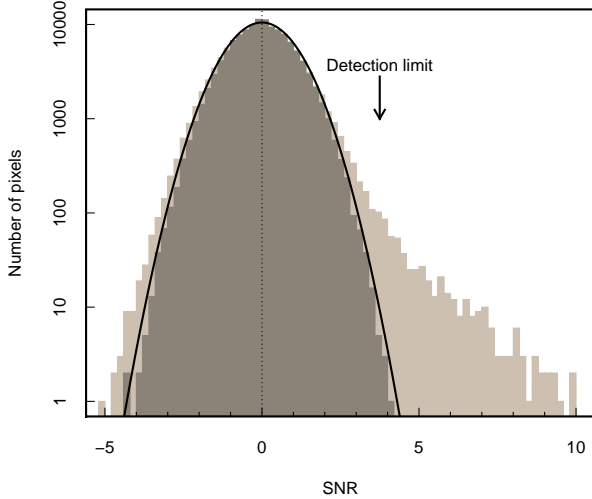
**Figure 2.** Histogram of values in the SCUBA–2 $450\mu$m signal-to-noise ratio map (Fig. 1), indicating the characteristic positive tail due to the presence of real astronomical sources. The solid line is a Gaussian centred at zero with a width of $\sigma = 1$, and the darker shaded histogram shows the histogram of pixel values in a map constructed by inverting a random 50% of the input scans; we use this for simulations of completeness, described in §2.3. Our detection limit is chosen to be $\sigma = 3.75$, which yields a reasonably complete and reliable catalogue (see §2.3). Note that the 'real' map noise distribution is slightly wider than expected for pure Gaussian noise; this is due to slight 'ringing' around bright sources after convolution with the beam.

The sky opacity at JCMT has been obtained by fitting extinction models to hundreds of standard calibrators observed since the commissioning of SCUBA–2 (Dempsey et al. 2012). The optical depth in the $450\mu$m band was found to scale with the Caltech Submillimetre Observatory (CSO) 225 GHz optical depth as: $\tau_{450} = 26.0(\tau_{225} - 0.0196)$. Note that this scaling is slightly different from the original SCUBA relations (see Archibald et al. 2002; Dempsey et al. 2012).

Filtering of the time-series is performed in the frequency domain, with band-pass filters equivalent to angular scales of $2'' < \theta < 120''$ (i.e. frequencies of $f = v/\theta$, where $v$ is the scan speed). The reduction also includes the usual filtering steps of spike removal ($>10\sigma$ deviations in a moving boxcar) and DC step corrections. Throughout the iterative map making process, bad bolometers (those significantly deviating from the model) are flagged and do not contribute to the final map. Maps from independent scans are co-added in an optimal stack using the variance of the data contributing to each pixel to weight spatially aligned pixels. Finally, since we are interested in (generally faint) extragalactic point sources, we apply a beam matched filter to improve point source detectability, resulting in a map that is convolved with an estimate of the $450\mu$m beam. The average exposure time over the nominal 3 arcminute daisy mapping region (in practice there is usable data beyond this) is approximately 10 ksec per $2'' \times 2''$ pixel.

## 2.2 Flux calibration

The flux calibration of SCUBA–2 data has been examined by analysing all flux calibration observations since Summer 2011 until the date of observation. The derived beam-matched flux conversion factor (FCF) has been found to be reasonably stable over this period, and the average FCFs agree (within error) to those derived

from the subset of standard calibrators observed on the nights of the observations presented here. Therefore we have adopted the canonical calibration of $\mathrm{FCF}_{450} = 540 \pm 65\,\mathrm{Jy\,beam^{-1}\,pW^{-1}}$ here. A correction of $\sim$10% is included in order to compensate for flux lost due to filtering in the blank-field map. This is estimated by inserting a bright Gaussian point source into the time stream of each observation to measure the response of the model source to filtering.

## 2.3 Maps and source detection

We present the $450\mu$m signal-to-noise ratio map of the COSMOS/CANDELS field in Fig. 1. For comparison, we also show a *Herschel* SPIRE $500\mu$m map of the same region to illustrate the gain in resolution that JCMT/SCUBA–2 offers at similar wavelengths[4]. The $450\mu$m map has a radially varying sensitivity, which is nearly uniform over the central $3'$ (the nominal mapping area) and smoothly increases in the radial direction as the effective exposure time decreases for pixels at the edge of the scan pattern, which have fewer bolometers contributing to the accumulated exposure. The total area of the map considered for source extraction is $140\,\mathrm{arcmin}^2$, where the rms noise is below $5\,\mathrm{mJy\,beam^{-1}}$. A histogram of pixel values in the $\sigma_{450} \leqslant 5\,\mathrm{mJy\,beam^{-1}}$ region is shown in Fig. 2.

To identify extragalactic point sources, we search for pixels in the (beam convolved) signal-to-noise ratio map with values $>\Sigma_{\mathrm{thresh}}$. If a peak is found, we record the peak-pixel sky coordinate, flux density and noise, mask-out a circular region equivalent to $\simeq 1.5\times$ the size of the $8''$ beam at $450\mu$m, reduce $\Sigma_{\mathrm{thresh}}$ by a small amount and then repeat the search. The floor value, below which we no longer trust the reality of 'detections' is chosen to be the signal-to-noise level at which the contamination rate due to false detections (expected from pure Gaussian noise) exceeds 5%, corresponding to a significance of $\sigma\approx 3.75$. We detect 60 discrete point sources in this way, and these are identified in Fig. 1. Note that the map is far from confused, with an average source density equivalent to $6 \times 10^{-3}\,\mathrm{beam^{-1}}$. We project that the confusion limit is at $\sim 1\,\mathrm{mJy\,beam^{-1}}$

Completeness is estimated by injecting a noise model with artificial point sources. To create maps with no astronomical sources but approximately the same noise properties of the real map, we generate jackknife realisations of the map where, in each fake map, a random half of individual scans have their signal inverted before co-addition (e.g. Weiss et al. 2009). Fig. 2 shows the equivalent histogram of signal-to-noise ratio values in the jackknife map, which demonstrates the clean removal of astronomical sources, and the similarity with pure Gaussian noise. The recovery rate of sources as a function of input flux and local noise gives the completeness function: $10^5$ fake sources in batches of 10 are inserted into the jackknife map, where each source selected from a uniform flux distribution $1 < (S_{450}/\mathrm{mJy}) < 40$. The 2-dimensional completeness function is shown in Fig. 3.

In addition to the completeness correction, this technique allows us to estimate the noise-dependent flux boosting that occurs for sources with true fluxes close to the noise limit of the map, and

---

[4] The *Herschel* map was made from the Level 2.5 processed data products downloaded from the public *Herschel* Science Archive. The data were co-added with sky coverage used as an estimator for image noise level, and re-binned into the SCUBA–2 image reference frame, using nearest-neighbour sampling. The $1\sigma$ noise level of this SPIRE map (including confusion) is $6.2\,\mathrm{mJy\,beam^{-1}}$

so we can construct an equivalent 'surface' in the noise–(measured) flux plane that can be use to de-boost the fluxes measured for point sources in the real map (Table 1). The typical de-boosting correction is $\mathcal{B} <10\%$. Finally, the source detection algorithm is applied to each of the jackknife maps with no fake sources injected in order to evaluate the false positive rate, which we find to be 5%, in agreement with the false detection rate expected for a map of this size assuming fluctuations from pure Gaussian noise.

A test for any bias in the recovery and correction of the source counts was performed in the following way. We populated the jack-knife maps with a model source count model (Béthermin et al. 2012b) down to a flux limit of $S_{450} = 0.01$ mJy. Sources were then extracted in exactly the same manner as the real data and completeness and flux boosting corrected as described above and then compared to the input distribution. This procedure was repeated 100 times and the average recovered source counts compared to the input model. The recovered differential and cumulative number counts were found to be consistent with the input number count realisations, indicating that our source detection and completeness corrections are not significantly biased.

## 3 ANALYSIS

### 3.1 Number counts of 450μm emitters

In Table 1 and Fig. 4 we present the number counts at 450μm, corrected for flux boosting and incompleteness. The differential counts are well-described by a Schechter function:

$$\frac{dN}{dS} = \left(\frac{N'}{S'}\right)\left(\frac{S}{S'}\right)^{1-\alpha} \exp\left(\frac{N'}{S'}\right), \qquad (1)$$

with $S' = 10$ mJy (fixed at a well-measured part of the flux distribution), $N' = (490 \pm 104)\,\text{deg}^{-2}$ and $\alpha = 3.0 \pm 0.7$.

At flux densities above 20 mJy, the number counts from this survey are complemented by the equivalent measurements from *Herschel* surveys, which survey wider areas at 500μm to shallower depths, and so find the rarer, bright sources (nearby galaxies, extremely luminous distant sources and gravitationally lensed galaxies) that are not present in our map (Clements et al. 2010; Negrello et al. 2010). We focus on two *Herschel* surveys; HerMES, which has obtained confusion limited maps reaching a detection limit of $S_{500} \approx 20$ mJy (Oliver et al. 2012) and the *Herschel*-ATLAS survey, which has mapped several hundreds of square degrees at a shallower depth (Eales et al. 2010). As Fig. 4 shows, our 450μm counts are in excellent agreement at $\approx$20 mJy where the *Herschel* and SCUBA–2 CLS survey flux distributions meet. Below *Herschel*'s confusion limit the 500μm galaxy number counts have been inferred statistically, by both stacking (Béthermin et al. 2012b) and pixel fluctuation analyses (Glenn et al. 2010), again indicating consistency with the directly measured 450μm number counts in approximately the same flux regime.

Recently, Chen et al. (2012) presented SCUBA–2 450μm observations of SMGs in the field of the lensing cluster A 370. The benefit of observing a lensing cluster is – provided a lens model is known – the ability to probe further down the luminosity function than would otherwise be possible for the same flux limit, with faint background sources boosted by the cluster potential. We compare the 'delensed' counts of 450μm emitters derived from 12 galaxies in the field of A 370 in Fig. 4, indicating broad agreement with our blank-field counts within the errors in the same flux range. After delensing, Chen et al. (2012) are able to probe slightly fainter than
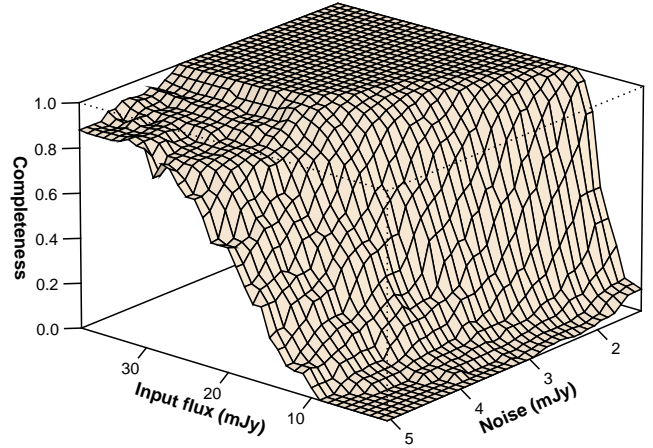


**Figure 3.** Completeness of the 450μm catalogue as a function of local noise and input flux based on input-and-recovery simulations using jackknife realisations of the map noise. Modelling the completeness as a 2-dimensional function is required due to the radially varying sensitivity in the map (Fig. 1). The same simulations allow us to estimate the difference between true (input) flux and recovered (i.e. observed) flux densities across the same parameter space, and we use this information to correct the number counts accordingly.

our catalogue, and the number counts at the 4.5 mJy level are also consistent with an extrapolation of our best fit Schechter function to the same limit.

### 3.2 Resolving the 450μm background light

What fraction of the CIB at 450μm have we resolved into galaxies? The integrated flux density of point sources detected at 450μm (corrected for completeness) is $I_\nu(450\mu m) = (7.4 \pm 0.7) \times 10^{-2}\,\text{MJy}\,\text{sr}^{-1}$. The absolute intensity of the CIB at 450μm measured by *COBE*–FIRAS is $I_\nu(450\mu m) = 0.47 \pm 0.19\,\text{MJy}\,\text{sr}^{-1}$, thus we have directly resolved $16 \pm 7\%$ of the CIB at 450μm (the uncertainty is dominated by the *COBE*–FIRAS measurement; Fixsen et al. 1998). For comparison, the deepest *Herschel* surveys have directly resolved 5–6% of the CIB at 500μm (Oliver et al. 2010; Béthermin et al. 2012a). We show the integrated brightness of the 450μm emitters, relative to the absolute intensity of the CIB in Fig. 4.

To measure the contribution to the CIB at 450μm by galaxies not formally detected in the SCUBA–2 map, but which are known to be infrared–bright galaxies, we stack the map at the position of 1600 galaxies selected from a catalogue generated from the *Spitzer*-COSMOS MIPS 24μm image of the same region (Sanders et al. 2007). First, we remove point sources from the 450μm map, using a point spread function (PSF) constructed by averaging the two dimensional profiles of sources detected at $>7\sigma$. This PSF was then normalised to the flux of each individual source in our catalogue, and subtracted from the map. This yields a residual map where the only flux (in addition to that of noise) is contributed by sources not in our catalogue. The 450μm is then stacked at the position of the 24μm sources, averaging the flux with a weight equivalent to the inverse of the variance of the map at each position.

The average 450μm flux density of 24μm sources with mean 24μm flux $\langle S_{24}\rangle = 0.19$ mJy is $\langle S_{450}\rangle = 2.2 \pm 0.4$ mJy. The resulting contribution to the 450μm background is $0.20 \pm$
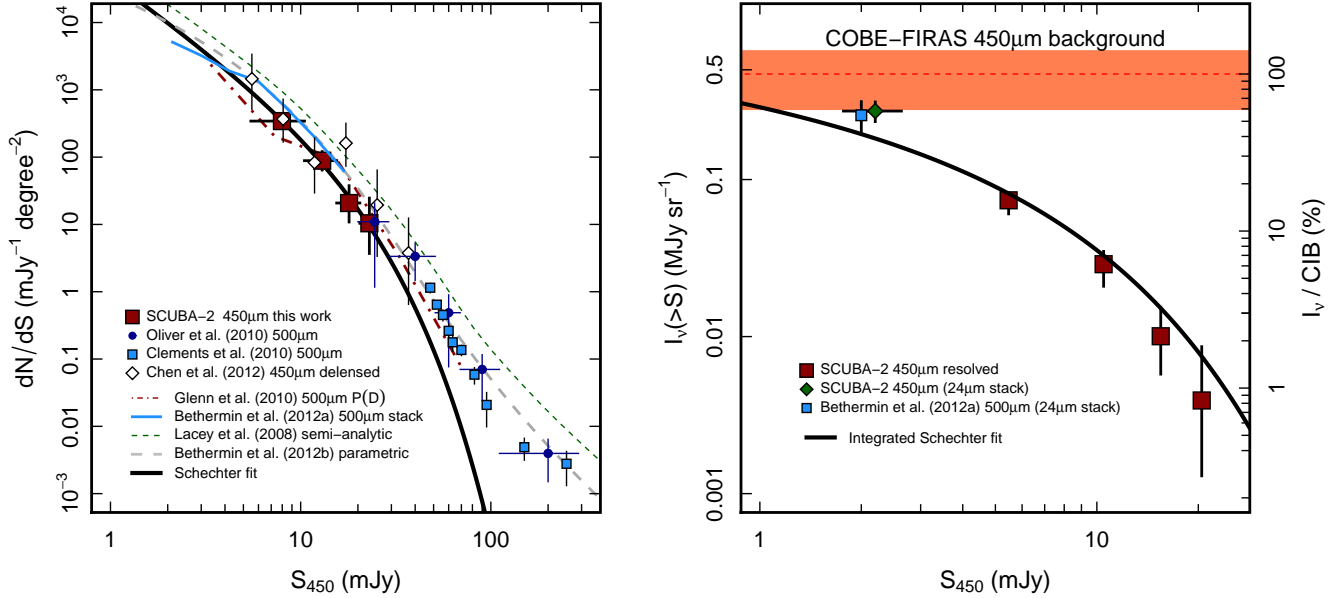
**Figure 4.** (left) Differential number counts of galaxies detected at $450\mu$m (error bars are derived from Poisson statistics). We compare the $450\mu$m counts to those measured recently by Chen et al. (2012) and by *Herschel* at $500\mu$m (Béthermin et al. 2012a; Glenn et al. 2010; Oliver et al. 2010; Clements et al. 2010), and to the predictions of a numerical model of galaxy formation (Baugh et al. 2005; Lacey et al. 2008) and a parametric model of the evolution of the infrared luminosity density of the Universe (Béthermin et al. 2012b). We fit the measured $450\mu$m counts with a Schechter function; the reason it fails to reproduce the shape of the $500\mu$m number counts (and those predicted by the models) at bright fluxes is because in this flux regime the counts have significant contributions from (a) bright local star-forming galaxies and (b) distant galaxies boosted to high observed flux by gravitational lensing; the SCUBA–2 map is too small to adequately sample these populations. Note – no $450\mu$m/$500\mu$m colour correction has been made to the $500\mu$m data. (right) Integrated surface brightness of $450\mu$m emitters relative to the CIB measured by *COBE*–FIRAS at $450\mu$m (Fixsen et al. 1998). The directly measured number counts are well-fitted by a Schechter function, the extrapolation of which agrees with the CIB derived from a stack of $24\mu$m-emitting galaxies not individually detected in the SCUBA–2 map. Thus, we directly resolve $16\pm7$% of the CIB measured by *COBE*–FIRAS into galaxies, with an additional $\approx40$% contributed by $24\mu$m-emitting galaxies not formally detected at $450\mu$m. We project that 100% of the CIB at $450\mu$m is recovered at a flux density of $S_{450} > 0.4$ mJy.

$0.04\,\mathrm{MJy\,sr^{-1}}$ (the uncertainty is $\sigma/\sqrt{N}$, with $\sigma$ the standard deviation in the stack and $N$ the sample size). A simple simulation was performed to test whether the stacking methodology described above produces unbiased estimates of the submillimetre flux. The residual flux map was inverted (by multiplying by $-1$) and simulated sources were inserted using the derived PSF as a model, with the input fluxes of the fake sources set to $S_{450} = 10S_{24}$ up to a maximum of $S_{450} = 5$ mJy. The positions were set to the $24\mu$m catalogue positions, rotated 90 degrees about the map centre, thus preserving clustering information. The stacking procedure was then repeated as for the real catalogue. The mean input flux was $S_{450} = 1.8$ mJy per source, and the recovered stacked flux was $S_{450} = 1.0 \pm 0.5$ mJy. The recovered flux is slightly low compared to the input flux at the $1.5\sigma$ level, however this does not affect our conclusions, given the uncertainties in the $450\mu$m flux calibration and the absolute measured value of the CIB at $450\mu$m.

Excluding those detected as bright point sources, the $24\mu$m-selected galaxies contribute $(2.0 \pm 0.4) \times 10^{-1}\,\mathrm{MJy\,sr^{-1}}$, or $42 \pm 19$% of the CIB at $450\mu$m. Therefore, in addition to the directly detected sources, in total we can account for $58 \pm 20$% of the CIB at $450\mu$m using the SCUBA–2 map. Note that our stacked value is in good agreement with the background derived from a stack of $24\mu$m-emitters in *Herschel* $500\mu$m images (Béthermin et al. 2012b), and is also consistent with the intensity expected from an extrapolation of a Schechter function fit to the directly measured number counts (Fig. 4).

**Table 1.** Number counts of $450\mu$m-selected galaxies. $N$ indicates the raw number of galaxies in each bin ($\delta S_{450} = 5$ mJy), and the completeness ($\mathcal{C}$) and de-boosting ($\mathcal{B}$) corrections represent the mean corrections for galaxies in each bin (note that each galaxy is de-boosted individually, with the correction increasing for lower flux densities). Uncertainties in the differential counts are the $1\sigma$ confidence range assuming Poisson statistics (Gehrels 1986).

| $S_{450}$ (mJy) | $N$ | $dN/dS$ (mJy$^{-1}$ deg$^{-2}$) | $N(>S')^a$ (deg$^{-2}$) | $\langle\mathcal{C}\rangle^b$ | $\langle\mathcal{B}\rangle^c$ |
|---|---|---|---|---|---|
| 8.0 | 41 | $343.0^{+62.6}_{-53.3}$ | $2313.4^{+339.7}_{-297.7}$ | 1.6 | 1.1 |
| 13.0 | 13 | $88.5^{+32.3}_{-24.2}$ | $598.5^{+172.4}_{-136.0}$ | 1.1 | 1.1 |
| 18.0 | 4 | $20.8^{+16.8}_{-9.9}$ | $155.9^{+94.7}_{-61.7}$ | 1.0 | 1.0 |
| 23.0 | 2 | $10.4^{+14.2}_{-6.7}$ | $52.0^{+71.0}_{-33.5}$ | 1.0 | 1.0 |

$^a$ $S'$ corresponds to the lower edge of the bin, i.e. $(S_{450} - 2.5)$ mJy
$^b$ average completeness correction applied
$^c$ average flux de-boosting correction applied

## 4  DISCUSSION

We compare our results to the phenomenological model of Béthermin et al. (2012b), who use a 'backwards evolution' parameterisation of the the infrared luminosity density (as traced by dusty star-forming galaxies; see also Lagache et al. 2004). The Béthermin et al. (2012b) model assumes that the star formation modes of galaxies can be either described as 'main sequence' (i.e. SFR scales

with stellar mass) or 'starburst', with spectral energy distributions defined by the latest stellar synthesis template libraries. The evolution of the luminosity functions of these two populations integrated over cosmic history provides good fits to the observed number counts of galaxies at 24, 70, 100, 160, 250, 350, 500, 850, 1100µm and 1.4 GHz (as well as integrated observables such as the evolution of the volume averaged star formation rate and cosmic infrared background). Here we confirm that the number counts of 450µm emitters predicted by the model is also in good agreement with the measured 450µm number counts in the flux range probed by our SCUBA–2 survey.

We also compare the measured counts to the GALFORM semianalytic model of galaxy formation (Cole et al. 2000; Baugh 2006; Lacey et al. 2008; Almeida et al. 2011). This prescription predicts the formation and evolution of galaxies within the $\Lambda$ CDM model of structure formation (Springel et al. 2005), and includes the key physics of the galaxy formation (and evolution) process: radiative cooling of gas within the dark matter halos, quiescent (by which we mean non-burst driven) star formation in the resultant discs, mergers, chemical enrichment of the stellar populations and intergalactic medium and feedback from supernovae and active galactic nuclei. As Fig. 4 shows, the numerical model slightly over-predicts the abundance of 450µm emitters in the flux range probed. Nevertheless, the reasonable agreement between the shape of the counts predicted by GALFORM and the data is encouraging for models of galaxy formation that aim to reproduce the full range of emission processes of galaxies at long wavelengths.

The 8 arcsec resolution of the 450µm SCUBA–2 map allows us to accurately identify the optical/near-infrared counterparts of the SMGs, and we have identified the most likely counterpart to the majority of 450µm sources in our sample (I. G. Roseboom et al. 2012 in prep). The wealth of legacy data available in the COSMOS field then provides the means to estimate the redshift distribution of the population. We have used 13 bands of optical/near-infrared photometry, including CFHT *ugri*, Subaru SuprimeCam *z'*, VISTA *YJHK*, *HST* F125W and F160W and *Spitzer* IRAC [3.6] and [4.5] to evaluate the photometric redshifts of all the identified galaxies (the typical $1\sigma$ uncertainty based on the confidence level of the template fit is $\delta z = 0.16$). The redshift distribution is shown in Fig. 5, indicating that the majority of our sample lie at $z < 3$, with a mean redshift of $\langle z \rangle = 1.3$ (a full analysis of the source identification and redshift distribution is to be presented in Roseboom et al. 2012 in prep). This is a clear indication that the 450µm selection is probing a lower redshift population than previous 850µm selected samples, which have typical redshifts of $\langle z \rangle = 2.2$ (e.g. Chapman et al. 2005; Wardlow et al. 2010). The shape of the redshift distributions predicted both by the phenomenological model and numerical model described above (for galaxies at the same flux limit) are also in good agreement with the measured distribution; both models predict little contribution from galaxies at $z > 3$ (although a high redshift 'tail' is present in both models).

Assuming the directly detected sources representing 16±7% of the CIB at 450µm are star-forming galaxies at $\langle z \rangle = 1.3$, then their total (rest-frame 8–1000µm) luminosities are in the ultraluminous class, $L_{IR} \approx 1.1 \times 10^{12} L_\odot$ (Chary & Elbaz 2001). If the galaxies contributing to the 24µm stack described in §3.3 lie in the same redshift range as the directly detected galaxies, then the majority (60%) of the CIB at 450µm is emitted by galaxies with $L_{IR} > 3.6 \times 10^{11} L_\odot$. This is broadly consistent with the picture that at $z \approx 1$, the star formation rate budget of the Universe is dominated by galaxies in the LIRG class, with star formation rates of
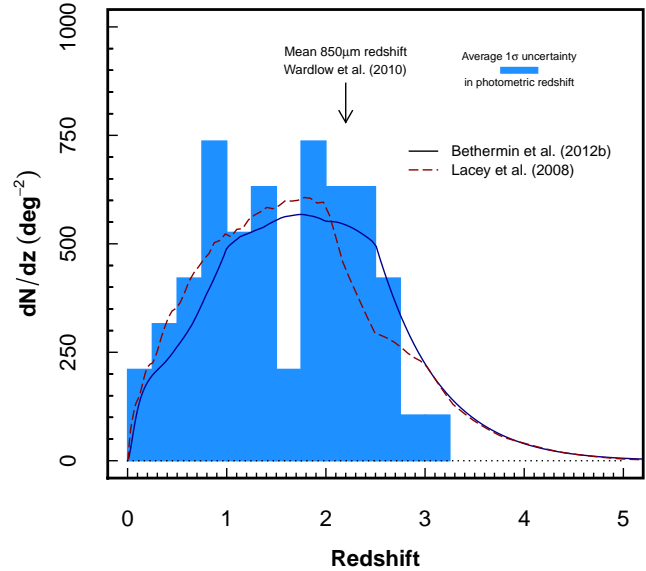


**Figure 5.** Redshift distribution of 450µm-selected SMGs in our sample (not corrected for completeness), derived from 13-band photometric redshift estimates (§3.4). The average redshift of the sample is $\langle z \rangle$=1.3, and the vast majority of the 450µm-selected SMGs lie at $z < 3$. For comparison, the average redshift of SMGs selected at 850µm is $z \approx 2.2$ (Wardlow et al. 2010), indicating the efficacy at which the 450µm selection samples a population of SMGs at lower redshift and therefore an important complement to any census of the dusty Universe. We compare the shape of the redshift distribution to the models of Béthermin et al. (2012b) and Lacey et al. (2008) shown in Fig. 4 for galaxies with $S_{450} > 5$ mJy (we have area-normalised both model distributions, since the observed redshift distribution contains no completeness correction). The average redshift and shape of both model distributions is in good agreement with observations, suggesting that – at this flux limit – there is little contribution from galaxies at $z > 3$.

order $10 \, M_\odot \, yr^{-1}$ (Dole et al. 2006; Rodighiero et al. 2010; Magnelli et al. 2011).

An extrapolation of the Schechter function fit to the directly measured number counts (which agrees well with the background at $S_{450} \approx 2$ mJy, derived from the stack of 24µm sources), implies that 100% of the CIB at 450µm should be recovered at $0.1 < S_{450} < 1.4$ mJy (the range accounting for the $1\sigma$ uncertainty of the absolute measured background; Fixsen et al. 1998), close to the SCUBA–2 confusion limit. If the galaxies responsible for this emission are at similar redshifts to the current 450µm sample (but below the sensitivity of the map and not contributing to the 24µm stack), then the majority of the remaining $\approx$40% of the CIB at 450µm is likely to be emitted by galaxies with $L_{IR} < 1.3 \times 10^{11} L_\odot$, implying galaxies star formation rates of a few tens of Solar masses per year. However, we cannot as yet rule out what fraction of the remaining CIB light might be emitted by faint 450µm emitters at higher redshifts; note that a galaxy with $S_{450} \approx 2$ mJy at $z > 2$ has a typical luminosity of $L_{IR} > 5.5 \times 10^{11} L_\odot$ (Chary & Elbaz 2001), again indicating the importance of LIRG-class galaxies in the cosmic infrared budget. Characterizing the high redshift tail of the 450µm population is an important next step.

## 5 SUMMARY

The SCUBA–2 camera on the 15 m JCMT repesents the state-of-the-art in panoramic submillimetre imaging, and has recently begun

scientific observations in earnest. In this paper we have presented results from the first deep, blank-field cosmological map at $450\mu$m ($\sigma_{450} = 1.3$ mJy); part of the SCUBA–2 Cosmology Legacy Survey, the largest of the seven JCMT Legacy Surveys. Using a $450\,\mu$m map of the well-studied extragalactic COSMOS/CANDELS field, we have

(i) made the first unbiased, blank-field determination of the number counts of galaxies at $450\mu$m, at a flux density limit of $S_{450} > 5$ mJy. This probes below the confusion limit of *Herschel*, complementing the number counts measured at fluxes above 20 mJy over wider areas in major *Herschel* submillimetre surveys;

(ii) measured the contribution of these galaxies to the cosmic infrared background at $450\mu$m: we resolve 16% of the CIB into individual galaxies. The ability of SCUBA–2 to 'pin-point' the galaxies responsible for the emission of the CIB is a critical step in understanding the properties of the galaxies that are forming the majority of stars in the Universe at this epoch;

(iii) an additional $\approx$40% of the CIB can be recovered in the SCUBA–2 map by stacking *Spitzer* MIPS-detected $24\mu$m emitters. Using this analysis we estimate that the majority ($\approx$60%) of the CIB at $450\mu$m is emitted by galaxies with $S_{450} > 2$ mJy;

(iv) a preliminary analysis of the redshift distribution of the $450\mu$m emitters (based on high-quality photometric redshifts available for this field) imply that the typical redshift of galaxies with $S_{450} > 5$ mJy is $\langle z \rangle = 1.3$, with the majority lying at $z < 3$. The typical luminosity of galaxies in our sample are estimated to be in the ultraluminous class, with $L_{IR} > 10^{12}$L$_\odot$. If the galaxies contributing to the statistical stack of $24\mu$m emitters described above are at a similar redshift, then we project that the majority of the CIB at $450\mu$m is emitted by 'LIRG' class galaxies with $L_{IR} > 1.3 \times 10^{11}$L$_\odot$.

These are the first results of the S2CLS. The final goal of the survey will be to map a quarter of a square degree to $\sigma_{450} = 1.2$ mJy, and a wider, ten square degree area to $\sigma_{850} = 1.5$ mJy, yielding $>10^4$ SMGs with which to (a) determine the submillimetre luminosity function and its evolution over cosmic time; (b) search for the rarest, most luminous SMGs at high-$z$; (c) resolve the $450\mu$m background; (d) accurately measure the clustering properties of SMGs and determine their typical environments (including rare protoclusters) and (e) build-up the large samples required to properly relate SMGs to other star-forming (ultraviolet/near-infrared selected) populations at $z \sim 2$ and thus gain further insight into SMGs' role in the overall history of galaxy evolution.

**REFERENCES**

Almeida, C., et al., 2011, MNRAS, 417, 2057
Archibald, E. N., et al., 2002, MNRAS, 336, 1
Aretxaga, I., et al., 2007, MNRAS, 379, 1571
Austermann, J. E., et al., 2010, MNRAS, 401, 160
Barger, A. J., et al., 1998, Nature, 394, 248
Baugh, C. M., et al., 2005, MNRAS, 356, 1191
Béthermin, M., et al., 2012a, A&A, 542, 58
Béthermin, M., et al., 2012b, ApJ, 757, L23
Blain, A. W., Smail, I., Ivison, R. J., & Kneib, J.-P. 1999, MNRAS, 302, 632
Chapman, S. C., Blain, A. W., Smail, I., & Ivison, R. J. 2005, ApJ, 622, 772
Chary, R., Elbaz, D., 2001, ApJ, 556, 562
Chen, C.-C., Cowie, L. L., Barger, A. J., Casey, C. M., Lee, N., Sanders, D. B., Wang, W.-H., Williams, J. P. 2012, arXiv:1209.4377
Clements, D. L., et al., 2010, A&A, 518, 8
Cole, S., Lacey, C. G., Baugh, C. M., Frenk, C. S., 2000, MNRAS, 319, 168
Coppin, K. E. K., et al., 2006, MNRAS, 372, 1621
Coppin, K. E. K., et al., 2008, MNRAS, 389, 45
Davé, R., Finlator, K., Oppenheimer, B. D., Fardal, M., Katz, N., Keres, D., Weinberg, D. H., 2010, MNRAS, 404, 1355
Dempsey, J. T., et al., 2012, SPIE Conference series 8452, Millimetre, Submillimetre and Far-infrared Detectors and Instrumentation for Astronomy VI, arXiv1208.4622
Devlin, M. J., et al., 1999, Nature, 458, 737
Dole, H., et al., 2006, A&A, 451, 417
Dunlop, J. S., et al., 2004, MNRAS, 350, 769
Dunlop, J. S., 2011, Galaxy evolution: Infrared to millimeter wavelength perspective. Proceedings of a conference held at Guilin, China 25-29 October 2010. Edited by W. Wang, J. Lu, Z. Luo, Z. Yang, H. Hua, and Z. Chen. San Francisco: Astronomical Society of the Pacific, 209
Eales, S., et al., 2010 PASP, 122, 499
Fixsen, D. J., Dwek, E., Mather, J. C., Bennett, C. L., & Shafer, R. A., 1998, ApJ, 508, 123
Gehrels, N., 1986, ApJ, 303, 336
Glenn, J., et al., 2010, MNRAS, 409, 109
Griffin, M. J., et al., 2010, A&A, 518, L3
Grogin, N. A., et al., 2011, ApJS, 197, 35
Hainline, L. J., et al., 2011, ApJ, 740, 96
Hauser, M. G., & Dwek, E., 2001, ARA&A, 39 249
Hickox, R. C., et al., 2012, MNRAS, 421, 284
Holland, W., et al., 2006, Millimeter and submillimetre Detectors and Instrumentation for Astronomy III. Edited by Zmuidzinas, J., Holland, W. S., Withington, S., Duncan, W. D., Proceedings of the SPIE. 6275
Hughes, D. H., et al., 1998, Nature, 394, 241
Ivison, R. J., Smail, Ian, Barger, A. J., Kneib, J.-P., Blain, A. W., Owen, F. N., Kerr, T. H., Cowie, L. L., 2000, MNRAS, 315, 209
Ivison, R. J., et al., 2002, MNRAS, 337, 1

Ivison, R. J., et al., 2005, MNRAS, 364, 1025

Ivison, R. J., et al., 2010, MNRAS, 404, 198

Jenness, T., et al., 2011, Astronomical Society of the Pacific Conference Series, Astronomical Data Analysis Software and Systems XX, 442, 281

Knudsen, K. K., van der Werf, P. P. & Kneib, J.-P., 2008, MNRAS, 384, 1611

Koekemoer, A. M., et al., 2011, ApJS, 197, 36

Lacey, C. G., Baugh, C. M., Frenk, C. S., Silva, L., Granato, G. L., Bressan, A., 2008, MNRAS, 385, 1155

Magnelli, B., Elbaz, D., Chary, R. R., Dickinson, M., Le Borgne, D., Frayer, D. T., Willmer, C. N. A., 2011, A&A, 528, 35

Michałowski, M., Hjorth, J., Watson, D., 2011, A&A, 514, 67

Negrello, M., et al., 2010, Science, 330, 800

Nguyen, H. T., et al., 2010, A&A, 518, L5

Oliver, S. J., et al., 2010, A&A, 518, L21

Oliver, S. J., et al., 2012, The Herschel Multi-tiered Extragalactic Survey: HerMES. MNRAS, 424, 1614

Pascale, E., et al., 2008, ApJ, 681, 400

Pilbratt, G. L., et al., 2010, A&A, 518, 1

Puget, J.-L., et al., 1996, A&A, 308, L5

Rodighiero, G., et al., 2010, A&A, 515, 8

Sanders, D. B., et al., 2007, ApJS, 172, 86

Scoville, N., et al.,2007, ApJS, 172, 1

Smail, I., Ivison, R. J., & Blain, A. W., 1997, ApJ, 490, L5

Smail, I., Ivison, R. J., Blain, A. W., Kneib, J.-P., 2002, MNRAS, 331, 495

Springel, V., et al., 2005, Nature, 435, 629

Swinbank, A. M., et al., 2006, MNRAS, 371, 465

Wardlow, J. L., et al.,2011, MNRAS, 415, 1479

Weiss, A., et al., 2009, ApJ, 707, 1201